New synthetic glass-based supplementary cementitious materials derived from basalt composition

Mohammad I.M. Alzeer [a,*], Christopher Cheeseman [b], Paivo Kinnunen [a,**]

[a] *Fibre and Particle Engineering Research Unit, University of Oulu, Pentti Kaiteran katu 1, 90014, Oulu, Finland*
[b] *UKCRIC Advanced Infrastructure Materials Laboratory, Department of Civil and Environmental Engineering, Imperial College London, SW7 2BU, UK*

ARTICLE INFO

ABSTRACT

The cement industry faces an increasing demand for new supplementary cementitious materials (SCMs) as alternative to slags and ashes, the sources of which are in continuous depletion. This study reports on the characteristics of synthetic aluminosilicate glasses derived from basalt composition (BGs) as new SCMs. The pozzolanic activity of the developed glasses as well as their influence on the hydration kinetics, microstructure, and mechanical properties of blended cements are reported. The obtained results show that pastes containing BGs demonstrated faster hydration rate and higher compressive strength compared to those containing commonly applied granulated blast furnace slag (GBFS). In addition, the developed glasses demonstrated higher pozzolanic activity than GBFS as demonstrated form the measured amount of portlandite and strength activity index. The developed glasses can be obtained from earth abundant carbon-free raw materials as it is similar in composition to basalt. Therefore, this novel approach has potential to provide low-carbon cementitious binders for the concrete industry.

1. Introduction

Reducing the greenhouse emissions associated with the production of Portland cement (PC) is an important research area. It is estimated that each kilogram of PC produces ~0.83 kg of carbon dioxide (CO_2) [1]. The 4.6 billion tons of PC produced in 2015 were responsible for 5–8% of total anthropogenic CO_2 emissions. PC production is expected to exceed 6 billion tons/year by 2050 and therefore urgent reductions in CO_2 emissions associated with cementitious binders are required [2]. Up to 60% of the CO_2 released during PC production is produced during clinker production from the decarbonation of limestone, with the remainder associated with fuels and electricity used during firing, milling and transportation [3]. Reducing the amount of CO_2 produced during PC clinker production has been optimized during the past few decades. The partial replacement of clinker in blended cements with supplementary cementitious materials (SCMs) is therefore now considered to be the most feasible approach to produce eco-efficient low-carbon cements [2]. The partial replacement of PC with SCMs can reduce CO_2 emissions by up to 40% without compromising the durability, strength and production costs of the material [3].

In addition to the ecological benefits, the presence of SCMs in blended cements has some desirable impacts on concrete, including enhanced long-term durability and improved mechanical properties [4]. The use of SCMs in concrete has therefore become common practice. However the current availability of conventional SCMs meets only 15% of the concrete industry demands [5]. Common SCMs

* Corresponding author.
** Corresponding author.
E-mail addresses: mohammad.alzeer@oulu.fi (M.I.M. Alzeer), paivo.kinnunen@oulu.fi (P. Kinnunen).

are granulated blast furnace slag (GBFS) and coal fly ash (FA). Supplies of FA are problematic due to the decrease in coal-fired power production in many countries. The increase in steel recycling as well as the move towards direct reduction of iron means that the supply of GBFS is also problematic [6]. Therefore, efforts have recently focused on finding new low-carbon sources of SCMs [7–9].

The performance of various naturally occurring materials including clays [5,10–12] and milled natural zeolites [13] as alternative SCMs have been reported. The use of calcined clay, in particular, has received much interest, and an example is limestone calcined clay cement (LC[3]) [5,14]. Aluminosilicate clays and zeolites are already utilized in other applications such as catalysis, adsorbents, paper manufacturing and this may militate against their large-scale use as SCMs in terms of cost and availability. Other industrial and agricultural wastes such as recycled granite quarry wastes [15], coal gangue [16], corn Stover ash [17], corn cob ash [18], and biomass ash [19], have also been investigated as alternative SCMs.

The common SCMs are mainly composed of glass and the average glass content in FA is ~60 wt% [20], and it is up to ~90% in GBFS [21]. This vitreous phase produces pozzolanic and/or hydraulic reactivity [22,23]. The main component in the glass phase of FA and GBFS is silica (the glass network former). The reactivity of silica is largely influenced by the presence of alkali and/or alkaline earth oxides (network modifiers) [22,23]. Alumina can act as both a network former when Al is present as tetrahedral or sometimes pentahedral substituent to silica in the amorphous aluminosilicate framework, or a modifier when present as extra-framework octahedral units [24,25]. The alkali or alkaline earth oxides cause disruption to the Si–O–Si bonds, thereby increasing the number of non-bridging oxygens (NBO), causing depolymerization of the glass network [24,26,27]. The reactivity of silicate and alumino-silicate glasses increases with the amount of network modifiers because this increases depolymerization. This explains the higher reactivity of Ca-rich FA (C-class with CaO wt% > 10%, according to the ASTM C618 standard) compared to Si-rich FA (F-class with CaO wt% < 10%, according to the ASTM C618 standard).

Since common SCMs are mainly composed of glass, efforts have been paid towards investigating the performance of both waste and synthetic glasses as potential alternative SCMs. Post-consumer waste glass is pozzolanic when mixed with PC [28–33]. However, applying waste glass as SCMs has many challenges; glass wastes are composed mainly of silica (≥70 wt% SiO_2), and therefore alkali-silica-reaction (ASR) commonly takes place in the concrete pore solution in presence of amorphous silica [34]. Hence, glass waste usually requires mechanical and/or chemical pre-treatments to overcome the problem associated with ASR. In addition, waste glass suffers from contamination and composition consistency of the waste stream. In this context, synthetic glasses are an attractive candidate SCM to partially replace cement because they can be synthesised with potentially zero raw-material related CO_2 emissions and their composition and characteristics can be optimized to enhance reactivity. Various studies have recently reported on the reactivity and characteristics of synthetic glasses that mimic the glassy phases present in FA and GBFS in terms of their phase and chemical composition in order to gain an insight on the reactivity of these commonly applied SCMs [22–24,26,35,36]. The development of synthetic glass as alternative SCMs to slags and ashes, and viable for large-scale production is of high significance and it is the topic of the present study.

Herein, we report on the performance of synthetic aluminosilicate glass with basalt composition as new SCMs. The reactivity of some synthetic glasses such as stone wool which is synthesised by melting and fiberizing basalt glass is associated with the hyper-quenching (very high cooling rate ~10^6 K/s). The basaltic glass presented here, on the other hand, is obtained at much lower cooling rate (~ 15 K/s) which is comparable to the cooling rate used for cementitious materials. The glass could also be prepared from combinations of abundant silicate minerals such as anorthite, olivine and wollastonite [37] and therefore, it has potential for large-scale production and utilization with low raw-material related CO_2 emissions as compared to PC. The synthesis of the glass presented in this study and its performance as alkali activated materials (AAMs) has recently been reported [38]. In this work, we investigated the hydration kinetics, hydration phases, pozzolanic reactivity and mechanical properties of blended cements containing the developed glass and compared their SCM performance to commonly applied GBFS.

Table 1
Chemical composition (wt%) of the synthesised glass and the other materials used in this study as measured by XRF, as well as particle size distribution.

Oxide	BG1	GBFS	CEM I 52.5R
SiO_2	39.8	34.3	24.0
Al_2O_3	20.5	9.1	2.1
Na_2O	5.4	0.6	–
MgO	8.7	9.8	0.7
CaO	18.6	37.9	69.0
Fe_2O_3	5.5	0.8	–
TiO_2	1.5	1.4	–
SO_3	–	2.8	2.3
K_2O	–	0.6	–
MnO	–	0.3	–
SrO	–	–	–
BaO	–	–	–
P_2O_5	–	–	–
Total	99.9	97.6	98.4
D50[a]	3.3	10.3	–

- not determined.
[a] Median particle size (μm).

2. Materials and methods

2.1. Materials

Silicon dioxide (99%, 325 mesh fused amorphous powder) was supplied by Alfa Aesar. Aluminum oxide (activated, neutral) and sodium carbonate (BioUltra, anhydrous ≥99.5%) were purchased form Sigma Aldrich. Calcium carbonate was supplied by VWR Chemicals, Magnesium carbonate (basic, extra pure) was supplied by Acros Organics, Fe_2O_3 (99.9% metal basis, Alfa Aesar), and TiO_2 (Anatase, 99.7% metals basis, Sigma Aldrich). CEM I 52.5R was supplied by Finnsementti, Finland and GBFS KJ400 was obtained from SSAB Raahe. The composition of CEM I, and GBFS are given in Table 1.

2.2. Glass preparation

The basaltic glass (BG) was synthesised with the composition given in Table 1 following the procedure previously reported [37]. In a typical batch, weighed amounts of the oxides (SiO_2, Al_2O_3, $MgCO_3$, $CaCO_3$, Na_2CO_3, Fe_2O_3, and TiO_2) were mixed manually and homogenized by milling in a rotary disc mill (Retsch RS 200) operated at 1400 rpm for 1 min. The mixture was then placed in a Pt crucible and melted in a Nabertherm high temperature furnace by heating to 1050 °C at 20 °C.min^{-1} where the sample was held for 2 h to ensure decarbonation. The temperature was then increased to 1600 °C at 10 °C.min^{-1} and held for 2 h. The melt was then casted on a water-cooled copper plate and cooled to room temperature. This glass was designated as BG1. Another batch of the glass was synthesised in the same way but was quenched in liquid N_2 (this was designated as BG2), in order to correlate the cooling rate with the reactivity of the glass formed glass. The glasses formed were milled with a rotary disc mill (Retsch RS 200) operated at 1400 rpm for 1 min and sieved through a 44 μm sieve.

2.3. Glass characteristics

Particle size distribution (PSD) was determined using a Beckman Coulter LS 13 320 laser diffraction particle size analyzer and the PSD data is presented in Fig. 1 and the median particle size (D50) in Table 1. X-ray fluorescence (XRF) analysis was conducted using AxiosmAX X-ray fluorescence spectrometer. X-ray diffraction (XRD) patterns were obtained using a Rigaku SmartLab 9 kW XRD diffractometer with Cu Kα radiation (Kα1 = 1.54056 Å; Kα2 = 1.54 Å) at a scan rate of 4°/min operated at 45 kV and 200 mA with phase identification determined using X'pert HighScore Plus (Malvern Panalytical Software).

2.4. Glass reactivity

The performance of the synthesised basalt glass (BG) as SCMs was evaluated in pastes prepared with a 0.5 water: solid ratio (w/s) with 30% replacement of PC. The results were compared with PC reference samples and pastes similarly prepared using GBFS. Pastes were prepared by mixing the PC and SCM manually for 1 min. Water was then added, and the paste mixed for 5 min. The pastes were cast into 20 × 20 × 80 mm molds and cured in a humid chamber (23 °C, 97% humidity). After 24 h, the pastes were demolded and kept in the humid chamber until testing. At the designated testing time (after 1, 7, and 28 days of hydration) a piece of each paste was broken and ground into powder, and the hydration stopped by immersing 1 g of the powder in 100 ml of isopropanol (≥99.7%, VWR chemicals) for 15 min. The sample was then filtered and washed thoroughly 3 times with isopropanol and dried at 40 °C for 30 min.

Calorimetry used 4 g of paste samples (70% PC, 30% SCMs) with 0.5 w/s ratio, with the heat recorded over 7 days using a TAM Air isothermal calorimeter at 23 °C, and H_2O was used as reference. The pastes were mixed ex-situ for 1 min using a laboratory shaker (Vortex-Genie 2). Field emission scanning electron microscopy (FESEM) analysis used a Zeiss ULTRA plus electron microscope
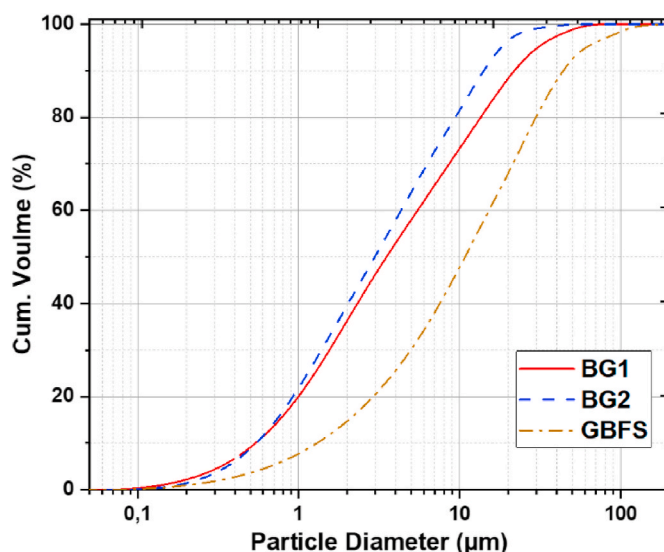

Fig. 1. Particle size distribution of the synthesised glasses and GBFS.

equipped with an electron dispersive detector (EDS) operated at 15 kV accelerating voltage. The samples were impregnated with epoxy resin and polished using diamond pastes followed by carbon coating (~8 nm layer of carbon) using a Vacuum Evaporator (JEE-420T, JEOL).

2.5. Pozzolanicity testing

2.5.1. Compressive strength

The compressive strength was measured using a Dartec testing machine with a force rate of 2.4 kN/min according to BS EN 196-1 standard. Three samples of each mix were tested, and the results are presented with the standard error (standard deviation/$\sqrt{n}$); where n is the number of samples. Strength activity index (SAI) values were determined according to EN 450-1 standard [39]. This defines the ratio of the compressive strength of pastes containing SCM to control PC samples. According to this standard, SAI values of $\geq$75% after 28 days of hydration indicate positive pozzolanic activity.

2.5.2. Amount of portlandite (CH%) and bound water (BW%)

Thermogravimetric analysis (TGA) data was obtained using a Precisa PrepASH 129 Thermogravimetric Analyzer. Approximately 0.5 g samples were heated from room temperature up to 1000 °C at a heating rate of 10 °C/min, under N_2 atmosphere. The TGA data indicates the amount of portlandite (CH%) from the weight loss between 414 and 520 °C using the tangential method. The amount of calcium carbonate (calcite, CC%) was determined as the weight % loss between 580 and 750 °C [15,40,41]. The amount of bound water (BW%) due to decomposition of the main hydrated phases, calcium silicate hydrate (C–S–H) and hydrated calcium aluminate (AFm) was then determined from the equation below [15]:

$$BW\% = \text{Total wt. loss at } 1000 \text{ °C} - (CH\% + CC\%)$$

3. Results and discussion

The formation of both BG1 and BG2 has successfully been achieved as evident from the X-ray diffraction pattern which shows an amorphous background in the range from 20° to 45° 2θ, without any crystalline phases as shown in Fig. 2. The shift of the background towards higher 2θ values for the BG1 indicates higher depolymerization of the glass network compared to the rapidly quenched glass (BG2). A similar trend was observed with aluminosilicate glasses that contains higher amount of network modifier [23]. However, both BG1 and BG2 were synthesised with the same composition and therefore the difference in the degree of polymerization between the two glasses might be linked to phase separation effects. The latter usually takes place during the glass synthesis, and is largely influenced by the cooling process, in which the network former (Si and/or Al oxides) separate from the network modifiers [37,42]. Detecting this separation on a sub-microscopic scale (<100 nm length scale) is challenging but could be achieved using high-resolution solid-state NMR techniques [42]. In this study, however, no major differences in the performance of both glasses as SCMs have been observed and therefore this feature has not been investigated further.

The hydration kinetics was studied by calorimetry as presented in Fig. 3. The results were normalized to the total binder weight in the mixture. The samples were mixed ex-situ and therefore the heat flow of the initial hydration peak could not be measured (Fig. 3a). The induction period appears the same for all the tested materials. The third stage (acceleration stage), which is apparent from the
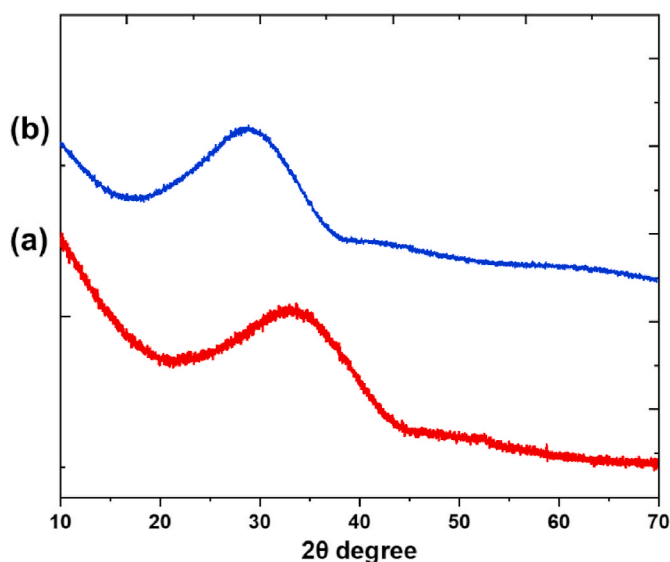

Fig. 2. XRD patterns of the synthesised glasses; (a)BG1 and (b) BG2.

main heat flow peak (Fig. 3a) is associated with the rapid nucleation and growth of C–S–H and portlandite. This was achieved after ~13 h of hydration when BG1, BG2 and GBFS were used as SCMs. This reflects that the initial and final setting time, which is determined from the heat flow curve of the third stage [43], are shortened when the glasses or GBFS are used as SCMs compared to the PC reference sample. The sharp rise in heat release for blends contained the BGs and GBFS (Fig. 3a) is attributed to the increase in the alkali solubility from these SCMs. It is known that SCMs influence the early hydration of PC by their pozzolanic reaction and physically by their filler effect. The filler effect of SCMs is a combination of three effects described as dilution, nucleation and accelerated hydration. The influence of SCMs on accelerating the early hydration of cement is well described elsewhere [44].

The total heat generated (Fig. 3b) reflects the enthalpies of formation of hydrated phases as well as the exothermic dissolution of phases from SCMs. The heat associated with the dissolution of portlandite and calcite is negligible [23]. Therefore, it could be assumed that the more heat generated reflects higher reactivity [23,43]. BG1 and BG2 show similar reactivity which is higher than GBFS. Nonetheless, it should be noted that the PSD of the glasses (BG1 and BG2) is smaller than GBFS (Fig. 1) which also contributes to their greater reactivity. The amount of cement used in the reference sample was similar to that used in other blends with SCMs to provide a more meaningful comparison. It can be seen from Fig. 3 that the hydration proceeds at a slightly faster rate for blends containing SCMs compared with the reference cement, but to a lower extent as seen from the higher total heat generated for the reference cement sample.

The weight loss % measured by TGA (Fig. 4) represents the evolution of bound water released from the formed hydrates. The main peak in the DTG (Fig. 4) at ~110 °C corresponds to water combined to C–S–H gel, while the shoulders at ~ 200 °C corresponds to other hydrated calcium aluminate phases (AFm) [15,23,40,41]. The peak at ~450 °C represent the dehydroxylation of portlandite while the peak at ~700 °C is associated with decarbonation of calcite [15,23,40,41]. The overall wt.% loss between 110 °C and 1000 °C increased with increasing curing time reflecting the increase in the hydrated phases formed. The amount of bound water (BW%) and the amount of portlandite (CH%) determined from TGA are presented in Fig. 5.

For all the pastes studied, the amount of bound water (BW) increases over time (Fig. 5a). After 7 days of hydration, blends with BG1 and BG2 show higher amount of BW compared to blends with GBFS. After 28 days of hydration the amount of BW for blends with BG1, BG2, and GBFS is comparable to the reference cement sample. The amount of BW indicates the progress of the hydration, rather than the degree of hydration, because the stoichiometry of the hydration reactions are not precisely known [45]. Thus, this indicates that the presence of the BG1 and BG2 accelerated hydration compared to other SCMs which is consistent with the calorimetry data (Fig. 3a).

Fig. 5b shows the amount of portlandite increased for all the pastes during the first seven days of hydration. Most of portlandite is produced during the first 7 days due to rapid hydration of alite but production continues up to 91 days due to the hydration of belite which usually occurs at a slower rate [46]. After 7 days hydration, all blends with SCMs show comparable amount of portlandite formed despite the variation of CaO content in the raw materials (Table 1). The PC reference sample contains the highest amount of portlandite compared with other blends that contains SCMs. This is because of the pozzolanic reactions that takes place in the presence of SCMs. After 28 days of hydration blends with BG1 and BG2 contain lower amount of portlandite compared to that with GBFS due to their higher pozzolanic reactivity. This is consistent with the results obtained by calorimetry (Fig. 3b).

Fig. 6 shows XRD data of pastes after 1 and 28 days of hydration. This confirms the formation of the phases identified by TGA/DTG (Fig. 4). All pastes show similar hydrated phases which are ettringite, portlandite, calcite, C–S–H, and belite (C_2S). The ZnO detected was used as an internal standard. For pastes with BG1, BG2, and GBFS a small peak at around 14° 2θ indicate the formation of hydrotalcite or calcium hemicarboaluminate (AFm) [47,48]. The XRD data shows that the addition of SCM resulted in no major mineralogical differences compared to that of the reference PC paste samples.

Fig. 7 shows the microstructure of the pastes obtained by SEM of polished cement pastes after 7 days hydration. On the grey scale distribution of backscattered SEM images, alite, portlandite, and C–S–H appear in a descending order of brightness and the pores/cracks appear black [49,50]. All pastes show bright grains of unreacted alite and precipitated portlandite. The micrographs show partially hydrated cement grains with a grey rim of inner hydration products (IP) surrounding a bright core of unreacted cement grain
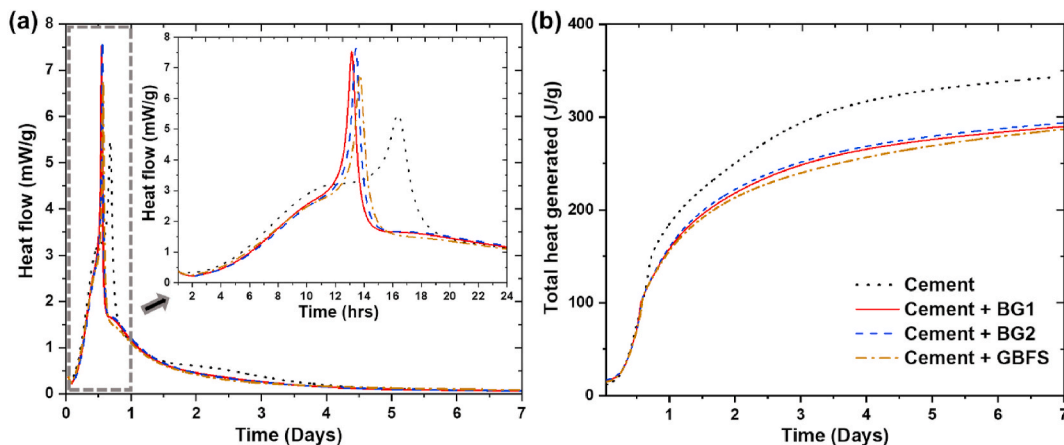

Fig. 3. Isothermal calorimetry results for blended cements with SCMs, (a) normalized heat flow (mW/g) and (b) cumulative heat generated (J/g).
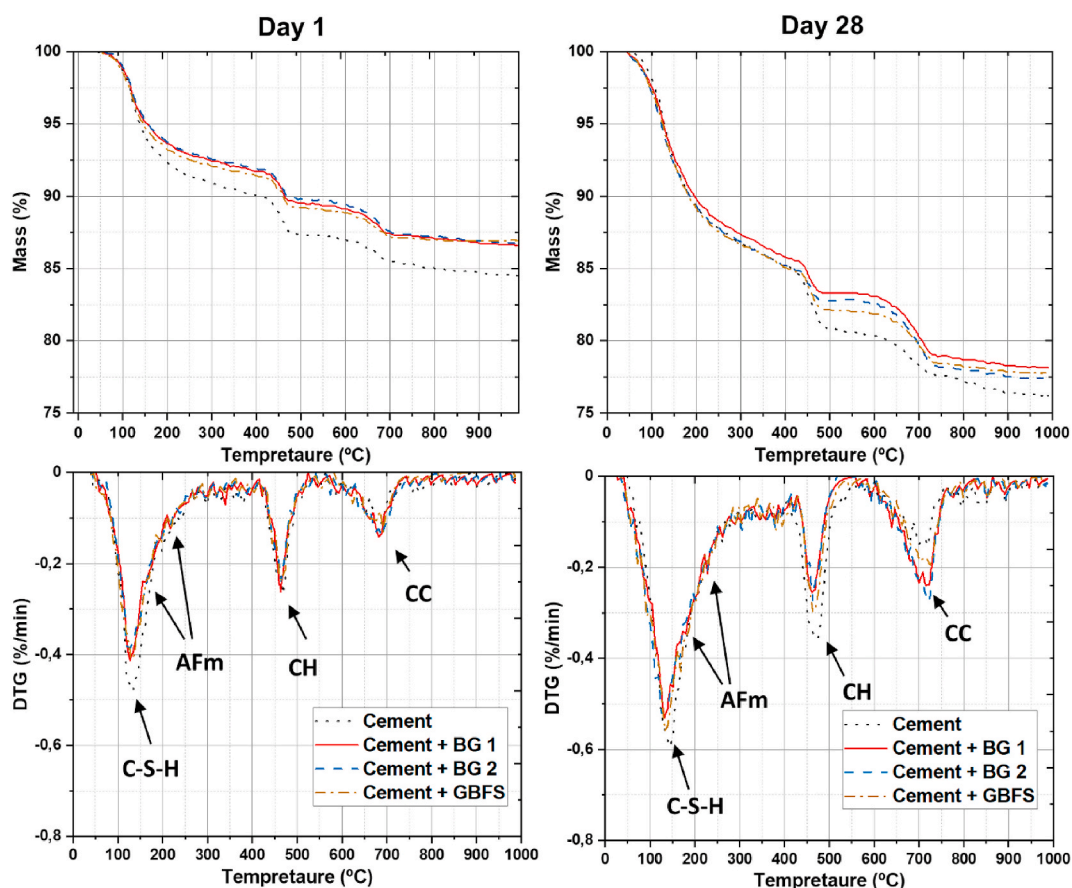
Fig. 4. TGA (top), and DTG analysis (bottom) of blends after 1 and 28 days of hydration. C–S–H: calcium silicate hydrate, AFm: hydrated calcium aluminate, CH: portlandite (Ca(OH)$_2$), CC: calcite (CaCO$_3$).

and outer products (OP) forming the matrix composed of C–S–H. Unreacted particles of the SCMs are also present (Fig. 7b and c) along with pores present in higher proportions in pastes with SCM compared to PC samples.

The chemical composition of hydration products in pastes are presented as atomic percentages in the Ca–Si–Al ternary compositional diagram obtained by EDS (Fig. 8). The data points are clustered within the C–S–H composition for all the prepared pastes [49–51]. Some points scattered towards higher Ca represent the composition of portlandite or calcite. The diagram also shows that other hydration phases such as (C, N)-A-S-H are formed, particularly for pastes containing BG1, and BG2.

The compressive strength and the strength activity index of the prepared pastes are presented in Fig. 9. Blends with SCMs, BG1, BG2, and GBFS, show low strength after 1 day of hydration (Fig. 9a). After 28 days hydration these pastes have slightly higher compressive strengths to the reference PC samples. Blended cements typically have lower early strength compared to PC samples but comparable or higher strength after longer periods of hydration. This is explained by changes in the phase assemblage, and consequently the microstructure, caused by the addition of SCM which results in a lower volume of hydrated phases and an increase in the total porosity as shown in Fig. 7 [23]. The strength activity index (SAI) after 28 days of hydration presented in Fig. 9b shows that pastes with BG1, BG2, and GBFS have a positive pozzolanic activity according to EN 450-1. The developed glasses show higher SAI value compared to GBFS indicating higher pozzolanic activity.

As mentioned above, the developed glass could be prepared from silicate minerals as the sole raw materials, and thus could be obtained with zero raw materials-related CO$_2$ (RM-CO$_2$) emissions. Compared to PC, these RM-CO$_2$ accounts for 60% of the total CO$_2$ emission associated with PC manufacturing. Additional CO$_2$ emission are associated with the energy consumption during glass melting. This energy has been estimated to be ~3.8 GJ/t, for a melting of an appropriate capacity of glass at 1600 °C, which is comparable to the energy used in PC production (~3.7 GJ/t) [37]. Furthermore, obtaining the developed glass from geological sources will provide a more consistent composition compared to commonly used SCMs such as coal FA whose chemical composition varies depending on the source of the coal and the combustion technology. This, in turn, influences the properties of the final blended cement.

4. Conclusion

This study reports the characteristics of aluminosilicate glass derived from Basalt composition (BGs) as new synthetic SCMs. The performance of the development glass as SCMs was evaluated and compared to other commonly applied SCMs such as GBFS. The
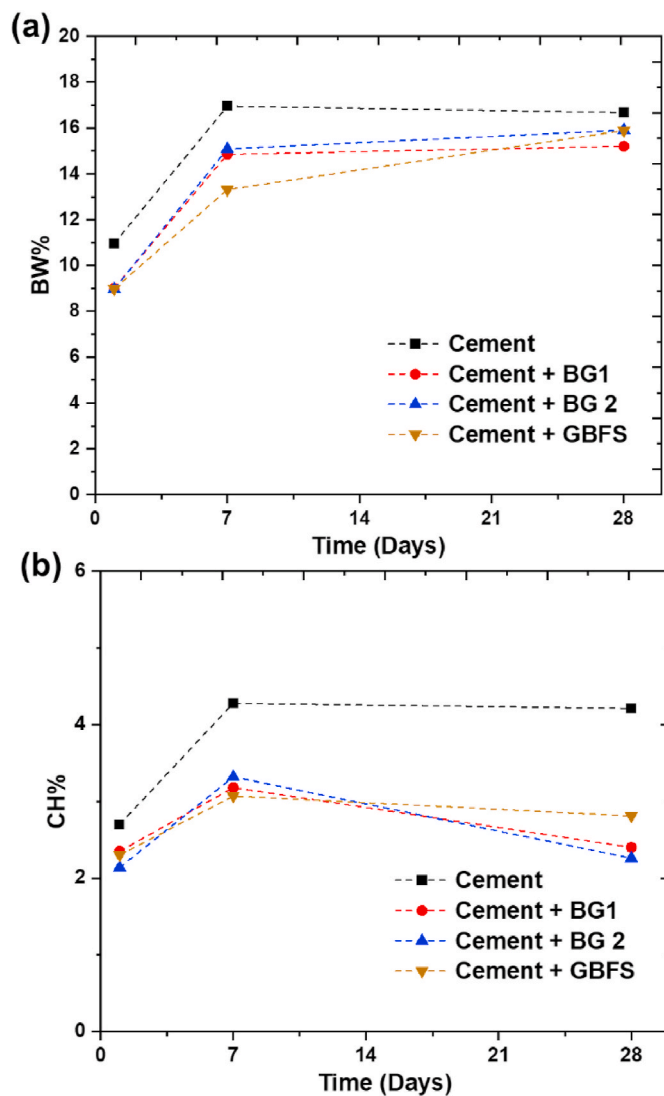
Fig. 5. (a) The amount of bound water (BW%) and (b) the amount of portlandite (CH%) in the studied blends, obtained by TGA.
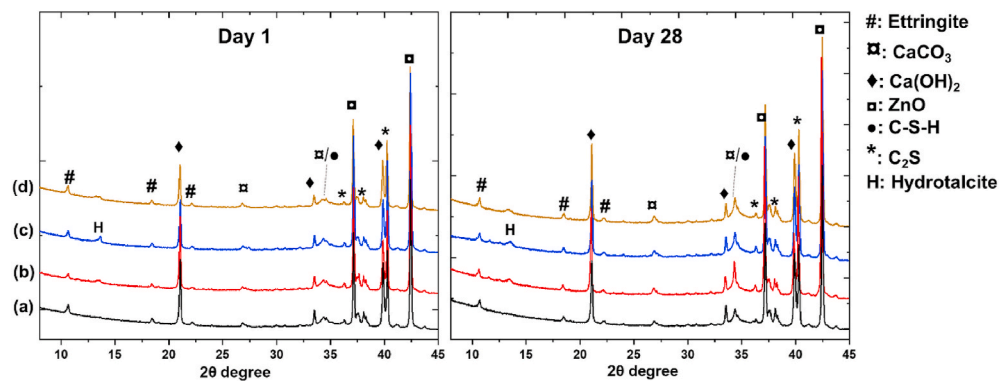

Fig. 6. XRD patterns of the studied pastes after 1 and 28 days of hydration. (a) Cement, (b) Cement + BG1, (c) Cement + BG2, (d) Cement + GBFS.
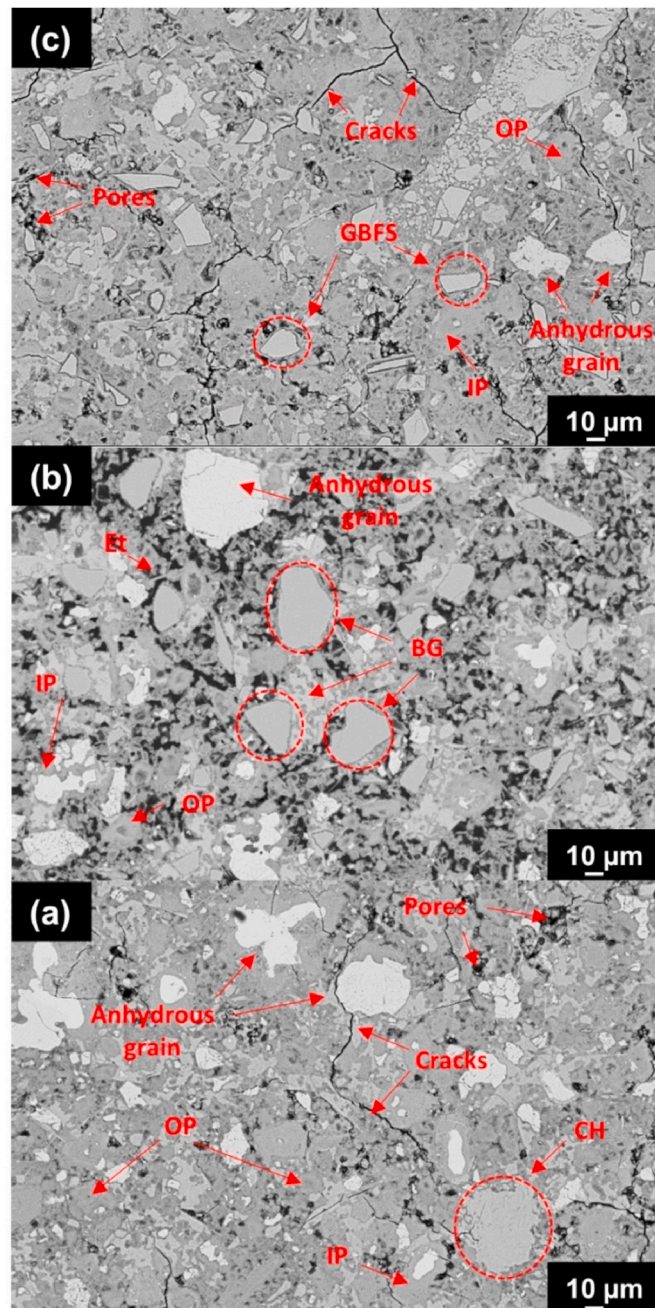
Fig. 7. Microstructure of the prepared pastes after 7 days of hydration. (a) cement, (b) cement + BG1, (c) cement + GBFS.

obtained results show that faster hydration rate was achieved for pastes with BGs compared to those containing GBFS. In addition, the pozzolanic reactivity of the developed BGs was found superior to GBFS as demonstrated form the measured amount of portlandite and strength activity index. Phase assemblage analysis shows that in addition to C–S–H, other Al-containing phases such as C-(N)-A-S-H and hydrotalcite are among the formed hydration phases for pastes containing BGs due to the high Al content in the developed glasses. The glasses demonstrate high potential to be used as an alternative SCMs to traditional slags and ashes, especially as they can be obtained from abundant naturally occurring mineral resources. The possibility of using silicate minerals as the sole raw material for glass synthesis allows SCMs production with low RM-CO_2 emissions, allowing the production of low-carbon blended cementitious binders.
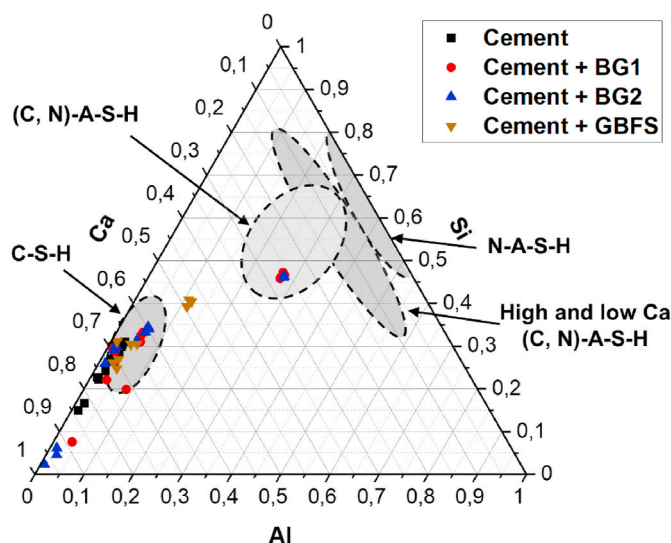
Fig. 8. Ca–Si–Al ternary compositional diagram for the prepared pastes. Phase identification circles were adapted from Ref. [51].
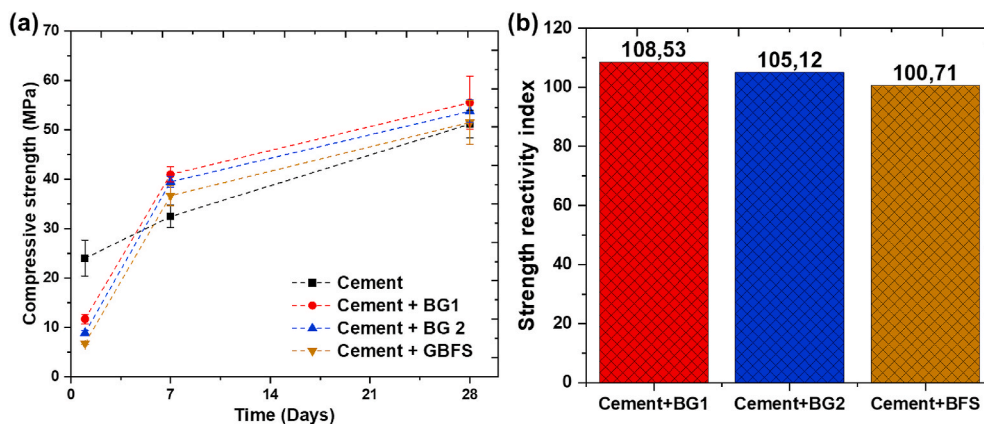

Fig. 9. Compressive strength (a), and strength reactivity index (b) of the prepared pastes.

CRediT authorship contribution statement

Mohammad I.M. Alzeer: Conceptualization, Formal analysis, Investigation, Methodology, Visualization, Writing – original draft, Writing – review & editing. **Christopher Cheeseman:** Conceptualization, Validation, Writing – review & editing. **Paivo Kinnunen:** Conceptualization, Formal analysis, Validation, Writing – review & editing, Supervision, Funding acquisition.

Declaration of competing interest

The authors declare that they have no known competing financial interests or personal relationships that could have appeared to influence the work reported in this paper.

Acknowledgments

References

[1] T. Stengel, P. Schießl, 22 - life cycle assessment (LCA) of ultra high performance concrete (UHPC) structures, in: F. Pacheco-Torgal, L.F. Cabeza, J. Labrincha, A. de Magalhães (Eds.), Eco-Effic. Constr. Build. Mater., Woodhead Publishing, 2014, pp. 528–564, https://doi.org/10.1533/9780857097729.3.528.

[2] K.L. Scrivener, V.M. John, E.M. Gartner, Eco-efficient cements: potential economically viable solutions for a low-CO2 cement-based materials industry, Rep. UNEP SBCI Work. GROUP LOW-CO2 ECO-Effic. Cem.-BASED Mater. 114 (2018) 2–26, https://doi.org/10.1016/j.cemconres.2018.03.015.

[3] J. Skibsted, R. Snellings, Reactivity of supplementary cementitious materials (SCMs) in cement blends, Cement Concr. Res. 124 (2019) 105799, https://doi.org/10.1016/j.cemconres.2019.105799.

[4] S.A. Miller, Supplementary cementitious materials to mitigate greenhouse gas emissions from concrete: can there be too much of a good thing? J. Clean. Prod. 178 (2018) 587–598, https://doi.org/10.1016/j.jclepro.2018.01.008.

[5] H. Maraghechi, F. Avet, H. Wong, H. Kamyab, K. Scrivener, Performance of Limestone Calcined Clay Cement (LC3) with various kaolinite contents with respect to chloride transport, Mater. Struct. 51 (2018) 125, https://doi.org/10.1617/s11527-018-1255-3.

[6] M.J. McCarthy, T. Robl, L.J. Csetenyi, 14 - recovery, processing, and usage of wet-stored fly ash, in: T. Robl, A. Oberlink, R. Jones (Eds.), Coal Combust. Prod. CCPs, Woodhead Publishing, UK, 2017, pp. 343–367, https://doi.org/10.1016/B978-0-08-100945-1.00014-9.

[7] M.C.G. Juenger, R. Snellings, S.A. Bernal, Supplementary cementitious materials: new sources, characterization, and performance insights, Cement Concr. Res. 122 (2019) 257–273, https://doi.org/10.1016/j.cemconres.2019.05.008.

[8] K. Sobolev, M. Kozhukhova, K. Sideris, E. Menéndez, M. Santhanam, Alternative supplementary cementitious materials, in: N. De Belie, M. Soutsos, E. Gruyaert (Eds.), Prop. Fresh Hardened Concr. Contain. Suppl. Cem. Mater. State—Art Rep. RILEM Tech. Comm. 238-SCM Work. Group 4, Springer International Publishing, Cham, 2018, pp. 233–282, https://doi.org/10.1007/978-3-319-70606-1_7.

[9] E. Aprianti S, A huge number of artificial waste material can be supplementary cementitious material (SCM) for concrete production – a review part II, J. Clean. Prod. 142 (2017) 4178–4194, https://doi.org/10.1016/j.jclepro.2015.12.115.

[10] R. Jaskulski, D. Jóźwiak-Niedźwiedzka, Y. Yakymechko, Calcined clay as supplementary cementitious material, Materials 13 (2020), https://doi.org/10.3390/ma13214734.

[11] E. Ghafari, S. Ghahari, D. Feys, K. Khayat, A. Baig, R. Ferron, Admixture compatibility with natural supplementary cementitious materials, Cement Concr. Compos. 112 (2020) 103683, https://doi.org/10.1016/j.cemconcomp.2020.103683.

[12] S. Papatzani, K. Paine, Inorganic and organomodified nano-montmorillonite dispersions for use as supplementary cementitious materials – a novel theory based on nanostructural studies, Nanocomposites 3 (2017) 2–19, https://doi.org/10.1080/20550324.2017.1315210.

[13] L.E. Burris, M.C.G. Juenger, Milling as a pretreatment method for increasing the reactivity of natural zeolites for use as supplementary cementitious materials, Cement Concr. Compos. 65 (2016) 163–170, https://doi.org/10.1016/j.cemconcomp.2015.09.008.

[14] K. Scrivener, F. Martirena, S. Bishnoi, S. Maity, Calcined clay limestone cements (LC3), Rep. UNEP SBCI Work. GROUP LOW-CO2 ECO-Effic. Cem.-BASED Mater. 114 (2018) 49–56, https://doi.org/10.1016/j.cemconres.2017.08.017.

[15] G. Medina, I.F. Sáez del Bosque, M. Frías, M.I. Sánchez de Rojas, C. Medina, Granite quarry waste as a future eco-efficient supplementary cementitious material (SCM): scientific and technical considerations, J. Clean. Prod. 148 (2017) 467–476, https://doi.org/10.1016/j.jclepro.2017.02.048.

[16] Y. Zhao, J. Qiu, Z. Ma, X. Sun, Eco-friendly treatment of coal gangue for its utilization as supplementary cementitious materials, J. Clean. Prod. (2020) 124834, https://doi.org/10.1016/j.jclepro.2020.124834.

[17] M. Shakouri, C.L. Exstrom, S. Ramanathan, P. Suraneni, J.S. Vaux, Pretreatment of corn stover ash to improve its effectiveness as a supplementary cementitious material in concrete, Cement Concr. Compos. 112 (2020) 103658, https://doi.org/10.1016/j.cemconcomp.2020.103658.

[18] M. Shakouri, C.L. Exstrom, S. Ramanathan, P. Suraneni, Hydration, strength, and durability of cementitious materials incorporating untreated corn cob ash, Construct. Build. Mater. 243 (2020) 118171, https://doi.org/10.1016/j.conbuildmat.2020.118171.

[19] M. Salvo, S. Rizzo, M. Caldirola, G. Novajra, F. Canonico, M. Bianchi, M. Ferraris, Biomass ash as supplementary cementitious material (SCM), Adv. Appl. Ceram. 114 (2015), https://doi.org/10.1179/1743676115Y.0000000043. S3–S10.

[20] C.R. Ward, D. French, Determination of glass content and estimation of glass composition in fly ash using quantitative X-ray diffractometry, in: Spec. Issue 2005 World Coal Ash Conf. 85, 2006, pp. 2268–2277, https://doi.org/10.1016/j.fuel.2005.12.026.

[21] E. Douglas, R. Zerbino, Characterization of granulated and pelletized blast furnace slag, Cement Concr. Res. 16 (1986) 662–670, https://doi.org/10.1016/0008-8846(86)90039-6.

[22] A. Schöler, F. Winnefeld, M.B. Haha, B. Lothenbach, The effect of glass composition on the reactivity of synthetic glasses, J. Am. Ceram. Soc. 100 (2017) 2553–2567, https://doi.org/10.1111/jace.14759.

[23] S. Kucharczyk, M. Zajac, C. Stabler, R.M. Thomsen, M. Ben Haha, J. Skibsted, J. Deja, Structure and reactivity of synthetic CaO-Al2O3-SiO2 glasses, Cement Concr. Res. 120 (2019) 77–91, https://doi.org/10.1016/j.cemconres.2019.03.004.

[24] S. Nie, R.M. Thomsen, J. Skibsted, Impact of Mg substitution on the structure and pozzolanic reactivity of calcium aluminosilicate (CaO-Al2O3-SiO2) glasses, Cement Concr. Res. 138 (2020) 106231, https://doi.org/10.1016/j.cemconres.2020.106231.

[25] Z. Wang, Y. Jiang, A. Baiker, J. Huang, Pentacoordinated aluminum species: new frontier for tailoring acidity-enhanced silica–alumina catalysts, Acc. Chem. Res. 53 (2020) 2648–2658, https://doi.org/10.1021/acs.accounts.0c00459.

[26] P.T. Durdziński, R. Snellings, C.F. Dunant, M.B. Haha, K.L. Scrivener, Fly ash as an assemblage of model Ca–Mg–Na-aluminosilicate glasses, Cement Concr. Res. 78 (2015) 263–272, https://doi.org/10.1016/j.cemconres.2015.08.005.

[27] J.F. Stebbins, Z. Xu, NMR evidence for excess non-bridging oxygen in an aluminosilicate glass, Nature 390 (1997) 60–62, https://doi.org/10.1038/36312.

[28] Z. Xie, Y. Xi, Use of recycled glass as a raw material in the manufacture of Portland cement, Mater. Struct. 35 (2002) 510–515, https://doi.org/10.1007/BF02483139.

[29] A. Khmiri, M. Chaabouni, B. Samet, Chemical behaviour of ground waste glass when used as partial cement replacement in mortars, Construct. Build. Mater. 44 (2013) 74–80, https://doi.org/10.1016/j.conbuildmat.2013.02.040.

[30] C. Shi, K. Zheng, A review on the use of waste glasses in the production of cement and concrete, Resour. Conserv. Recycl. 52 (2007) 234–247, https://doi.org/10.1016/j.resconrec.2007.01.013.

[31] A. Shayan, A. Xu, Performance of glass powder as a pozzolanic material in concrete: a field trial on concrete slabs, Cement Concr. Res. 36 (2006) 457–468, https://doi.org/10.1016/j.cemconres.2005.12.012.

[32] C. Shi, Y. Wu, C. Riefler, H. Wang, Characteristics and pozzolanic reactivity of glass powders, Cement Concr. Res. 35 (2005) 987–993, https://doi.org/10.1016/j.cemconres.2004.05.015.

[33] N. Schwarz, H. Cam, N. Neithalath, Influence of a fine glass powder on the durability characteristics of concrete and its comparison to fly ash, Cement Concr. Compos. 30 (2008) 486–496, https://doi.org/10.1016/j.cemconcomp.2008.02.001.

[34] L.M. Federico, S.E. Chidiac, Waste glass as a supplementary cementitious material in concrete – critical review of treatment methods, Sustain. Civ. Eng. Struct. - Durab. Concr. 31 (2009) 606–610, https://doi.org/10.1016/j.cemconcomp.2009.02.001.

[35] M. Moesgaard, D. Herfort, J. Skibsted, Y. Yue, Calcium aluminosilicate glasses as supplementary cementitious materials, Glass Technol. Eur. J. Glass Sci. Technol. 51 (2010) 183–190.

[36] P.T. Durdziński, C.F. Dunant, M.B. Haha, K.L. Scrivener, A new quantification method based on SEM-EDS to assess fly ash composition and study the reaction of its individual components in hydrating cement paste, Cement Concr. Res. 73 (2015) 111–122, https://doi.org/10.1016/j.cemconres.2015.02.008.

[37] P. Kinnunen, H. Sreenivasan, C.R. Cheeseman, M. Illikainen, Phase separation in alumina-rich glasses to increase glass reactivity for low-CO2 alkali-activated cements, J. Clean. Prod. 213 (2019) 126–133, https://doi.org/10.1016/j.jclepro.2018.12.123.

[38] M.I.M. Alzeer, H. Nguyen, C. Cheeseman, P. Kinnunen, Alkali-Activation of synthetic aluminosilicate glass with basaltic composition, Front. Chem. 9 (2021) 706, https://doi.org/10.3389/fchem.2021.715052.

[39] EN 450-1:Fly ash for concrete – Part 1: definition, specifications and conformity criteria. https://standards.iteh.ai/catalog/standards/cen/cc9c0d2c-6d67-4290-82ea-e5e99eb8abf0/en-450-1-2012, 2012.

[40] E. Gallucci, X. Zhang, K.L. Scrivener, Effect of temperature on the microstructure of calcium silicate hydrate (C-S-H), Cement Concr. Res. 53 (2013) 185–195, https://doi.org/10.1016/j.cemconres.2013.06.008.

[41] M. Torres-Carrasco, J.J. Reinosa, M.A. de la Rubia, E. Reyes, F. Alonso Peralta, J.F. Fernández, Critical aspects in the handling of reactive silica in cementitious materials: effectiveness of rice husk ash vs nano-silica in mortar dosage, Construct. Build. Mater. 223 (2019) 360–367, https://doi.org/10.1016/j.conbuildmat.2019.07.023.

[42] J.F. Stebbins, N. Kim, M.J. Andrejcak, P.M. Boymel, B.K. Zoitos, Characterization of phase separation and thermal history effects in Magnesium silicate glass fibers by nuclear magnetic resonance spectroscopy, J. Am. Ceram. Soc. 92 (2009) 68–74, https://doi.org/10.1111/j.1551-2916.2008.02844.x.

[43] A. Fernández-Jiménez, I. Garcia-Lodeiro, O. Maltseva, A. Palomo, Hydration mechanisms of hybrid cements as a function of the way of addition of chemicals, J. Am. Ceram. Soc. 102 (2019) 427–436, https://doi.org/10.1111/jace.15939.

[44] Z. Zhang, W. Chen, F. Han, P. Yan, A new hydration kinetics model of composite cementitious materials, Part 2: physical effect of SCMs, J. Am. Ceram. Soc. 103 (2020) 3880–3895, https://doi.org/10.1111/jace.17055.

[45] V. Kocaba, E. Gallucci, K.L. Scrivener, Methods for determination of degree of reaction of slag in blended cement pastes, Cement Concr. Res. 42 (2012) 511–525, https://doi.org/10.1016/j.cemconres.2011.11.010.

[46] K. Vessalas, P.S. Thomas, A.S. Ray, J.-P. Guerbois, P. Joyce, J. Haggman, Pozzolanic reactivity of the supplementary cementitious material pitchstone fines by thermogravimetric analysis, J. Therm. Anal. Calorim. 97 (2009) 71, https://doi.org/10.1007/s10973-008-9708-5.

[47] T. Runčevski, R.E. Dinnebier, O.V. Magdysyuk, H. Pöllmann, Crystal structures of calcium hemicarboaluminate and carbonated calcium hemicarboaluminate from synchrotron powder diffraction data, Acta Crystallogr. B 68 (2012) 493–500, https://doi.org/10.1107/S010876811203042X.

[48] P. Feng, C. Miao, J.W. Bullard, Factors influencing the stability of AFm and AFt in the Ca–Al–S–O–H system at 25°C, J. Am. Ceram. Soc. 99 (2016) 1031–1041, https://doi.org/10.1111/jace.13971.

[49] J.E. Rossen, K.L. Scrivener, Optimization of SEM-EDS to determine the C–A–S–H composition in matured cement paste samples, Mater. Char. 123 (2017) 294–306, https://doi.org/10.1016/j.matchar.2016.11.041.

[50] J.-I. Escalante-Garcia, J.H. Sharp, The chemical composition and microstructure of hydration products in blended cements, Scanning Electron Microsc. Cem. Concr. 26 (2004) 967–976, https://doi.org/10.1016/j.cemconcomp.2004.02.036.

[51] P. Perez-Cortes, J.I. Escalante-Garcia, Design and optimization of alkaline binders of limestone-metakaolin – a comparison of strength, microstructure and sustainability with portland cement and geopolymers, J. Clean. Prod. 273 (2020) 123118, https://doi.org/10.1016/j.jclepro.2020.123118.